Research Article

Sven Schröder*, Méabh Garrick, Anne-Sophie Munser and Marcus Trost

Spectral laser damage testing of optical materials

DOI 10.1515/aot-2017-0033
Received April 20, 2017; accepted June 1, 2017; previously published online July 19, 2017

Abstract: The spectral laser-induced damage of optical components was measured using a new instrument based on combining a laser-induced damage threshold (LIDT) testing procedure with angle-resolved light scattering and using a tunable optical parametric oscillator laser source. Tests on aluminum mirrors revealed a significant drop of the LIDT around 800 nm, which is not predicted by simple scaling laws. For near-infrared edge filters, remarkable changes in the LIDT around the band edge were observed, which are linked to the spectral variation of the field distribution in the interference coating.

Keywords: angle-resolved scattering; laser-induced damage; light scattering.

1 Introduction

Laser-induced damage of optical components is the limiting factor for the performance and lifetime of high-power optical systems. The laser-induced damage threshold (LIDT) of an optical element at a given wavelength is the highest operating fluence for which the probability of damage is zero. The LIDT depends on a number of parameters related to the light source (wavelength, pulse duration, pulse number) and the sample (dielectric properties, interface roughness, defects). As a result, determining reliable LIDT data requires careful and standardized measurement procedures.

The laser stability is not only limited by the intrinsic absorption of the materials involved but also strongly influenced by the field distribution, particularly for coatings, as well as extrinsic factors such as defects and contaminations [1]. These factors result in a strong wavelength dependence on the laser-induced damage threshold.

State-of-the-art laser-induced damage testing is usually performed at single wavelengths, typically those of technically relevant high-power lasers, such as Nd:YAG laser at its fundamental wavelength of 1064 nm and its higher harmonics (532 nm, 355 nm, 266 nm). An international standard has been developed, which describes systematic procedures to determine the laser-induced damage threshold of optical components [ISO 21254], and several groups have implemented LIDT testing procedures and have long-term experience in analyzing and interpreting the data [2–5].

Determining the LIDT at certain fixed wavelengths is highly relevant for many high-power applications. Yet, more and more applications require knowledge of the laser stability over larger spectral regions. One example is optical systems for tunable lasers like optical parametric oscillators (OPOs) or chirped mirrors for ultra-short laser pulses. Simple wavelength scaling laws [1] can be used to estimate the LIDT behavior in the region around the tested wavelength. They fail, however, as soon as the spectral dielectric properties of the component change significantly. This is basically true for any material and even more critical for interference coatings with strong changes of the field distribution in their spectral range of application. For these applications, the LIDT at one wavelength does not sufficiently allow performance predictions over the entire range of relevant wavelengths.

First, results of spectral scattering modeling and measurements of dielectric coatings revealed a tremendous change of the scattering characteristics even at wavelengths close to the central wavelength of the coating [6]. As light scattering is driven by the roughness properties of the interfaces, which do not depend on the wavelength if we ignore the slight shift of the relevant spatial frequency range with wavelength [7], as well as the field distribution inside the coating stack, this clearly suggests that the LIDT will also have a strong wavelength dependence.

Another issue is the influence of isolated defects onto the LIDT in existing standard setups. For some applications, it is interesting to check the homogeneity and the

***Corresponding author: Sven Schröder,** Fraunhofer Institute for Applied Optics and Precision Engineering, Albert-Einstein-Str. 7, 07745 Jena, Germany, e-mail: sven.schroeder@iof.fraunhofer.de
Méabh Garrick, Anne-Sophie Munser and Marcus Trost: Fraunhofer Institute for Applied Optics and Precision Engineering, Albert-Einstein-Str. 7, 07745 Jena, Germany

cleanliness of a sample before testing or even to know the LIDT on a defect site.

In this paper, we report on a study of the spectral dependence of laser-induced damage of different optical components ranging from metallic mirrors to interference coatings. In contrast to existing setups, we implemented our setup into an instrument for angle-resolved light-scattering measurements. The instrument allows us to (i) perform a scatter mapping of the sample before LIDT testing to localize inhomogeneities and defects, (ii) perform LIDT tests on selected positions on the sample, and (iii) use the highly sensitive scatter detector to study the degradation of the samples during irradiation even before ultimate damage occurs.

2 Experimental method

2.1 Definitions

Laser-induced damage is defined as any permanent laser-radiation-induced change in the characteristics of the surface or bulk of the specimen, which can be observed by any inspection technique discussed in (ISO 21254-1 [8]). The 0% LIDT of a component is the highest energy per unit area for which no damage is induced at or below the surface. For lasers with pulsed emission, the LIDT is typically measured in units of J/cm², known as the fluence per pulse. The fluence, F, is then essentially given by:

$$F = \frac{E}{A} = \frac{P_{pk}\tau}{A} \tag{1}$$

where E, is the measured pulse energy with peak power P_{pk}, at a given pulse duration τ, and A is the cross-sectional area of the beam. For a Gaussian beam, A and E are scaled to account for the non-uniform spatial and temporal profile of each pulse. As defined by ISO 11254-2 [9], the effective area A_{eff} and the pulse duration τ_{eff} are then:

$$A_{\text{eff}} = \frac{\pi d_{0.135}^2}{8} \tag{2}$$

$$\tau_{\text{eff}} = \frac{\sqrt{\pi}\tau_{0.135}}{2} \tag{3}$$

where $d_{0.135}$ and $\tau_{0.135}$ are the beam diameter and pulse duration as defined at 1/e² intensity level.

In our setup, a pyroelectric energy meter is used to measure the total pulse energy E_{tot}. Consequently, this quantity must also be scaled using Equation (3). The fluence for measurements in our instrument is thus:

$$F = \frac{4E_{\text{tot}}}{\sqrt{\pi}d_{0.135}^2} \tag{4}$$

2.2 Experimental setup

The experimental setup is shown in Figure 1. The instrument is based on a Sunlite EX optical parametric oscillator (OPO) (Continuum, San Jose, CA, USA) pumped with an injection seeded, frequency tripled Nd:YAG pump laser at 355 nm and followed by an optical parametric amplifier. The pulse length is 5 ns, and the repetition rate is 20 Hz. The tuning range of the OPO is 445 nm–1750 nm with a bandwidth of <0.1 nm over the entire spectral range and an output energy of up to 50 mJ. A frequency doubler can be used to generate radiation in the range between 225 nm and 445 nm. Detailed descriptions of the OPO instrument and the theory behind OPO operation are given in Ref. [10]. In addition to the spectrally selective prism outcouplers of the OPO, edge filters are used to remove out-of-band radiation when operating with the signal wave (445–710 nm) or the idler wave (710–1750 nm).

Two Glan-Taylor calcite polarizers in succession are used as variable attenuators to adjust the incident power. The broadband transmission of the polarizers (400–2200 nm, T: 85–90%), along with their high damage threshold of 20 J/cm² (λ: 1064 nm, τ: 10 ns, repetition rate: 10 Hz, beam diameter: 0.433 mm), allows for accurate energy adjustment across the entire wavelength range of up to two orders of magnitude. The relative long transmission length of the polarizers requires a particularly high-precision alignment in order to avoid lateral beam movement on the sample when rotating the polarizers to adjust the power.

A spatial filter consisting of two spherical focusing mirrors (diameter 50 mm, aluminum or silver with dielectric protective coating) and a pinhole (diameter 100 µm) is used to generate a clean beam.

A broadband beam splitter (90:10, T:R), was positioned at a slight angle, outcoupling the beam for beam diagnostics. Online pulse energy measurement is performed using a pyroelectric energy sensor converting the pulse energy into a voltage pulse with an amplitude proportional to the energy. Systematic beam profile measurements as a function of wavelength were performed and used as

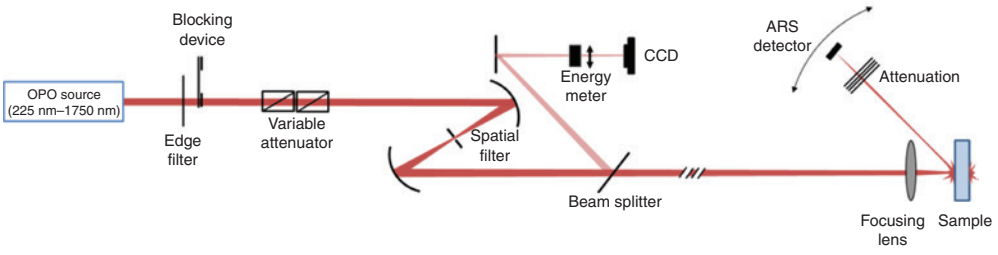

Figure 1: Setup for spectral laser-induced damage testing and angle-resolved light scattering measurements.

a guide for focal spot size, while the mounted CCD of the setup was merely used for monitoring changes in spatial profile during measurement campaigns.

The sample is mounted into a precision double goniometer system, which allows scanning the lateral position of the sample, the angle of incidence, and the scatter angle [8]. In contrast to a regular scatterometer setup, the incident beam is focused onto the sample (spot diameter ~100 μm) using an uncoated CaF_2 convex lens with an effective focal length of 100 mm. The lens is mounted to the outer structure of the goniometer and, thus, independent of the translation stage and the detector in order to keep the lens stationary when scanning the sample. During wavelength changes, the lens is refocused manually in order to retain the superposition of the focal point and the front surface of the sample. By focusing onto the sample, fluences of up to 10^3 J/cm^2 can be achieved. As mentioned above and discussed in more detail in Section 2.4, the actual diameter and the profile of the illumination spot on the sample slightly changes with the wavelength. The effective beam diameter measured using a CCD sensor placed in the focal plane varies between approximately 50 μm and 200 μm depending on the wavelength. This information is used for the calculation of the fluence as described in Section 2.1.

For highly sensitive light-scattering measurements, a photomultiplier tube is used as an angle-resolved scattering (ARS) detector, which can be scanned within the entire scattering sphere around the sample. During damage testing, absorptive neutral density filters are placed between the sample and the detector in order to facilitate high fluence irradiation of the sample while ensuring that scatter levels remain within the linearity range of the detector.

The combination of LIDT testing with *in situ* highly sensitive ARS analysis provides additional information. In particular, scanning the sample before, during, and after irradiation tests and measuring the scattering into selected angles is useful to (i) characterize the samples before damage testing, (ii) observe changes in the scattering properties during irradiation caused by changes of the structural and optical properties until, of course, potential fatal damage, (iii) classify irradiated sites into damaged and undamaged, as well as to assess the possible influence of preexisting sample inhomogeneities onto the results. Sample characterization before and after damage testing is, of course, performed with fluences far below the LIDT, usually in the range of mJ/cm^2.

2.3 Test procedures

2.3.1 Standard procedures: The instrument enables several parameters to be varied in order to systematically determine the spectral laser stability. This includes the incident wavelength, the lateral position of the sample with respect to the illuminating beam, the incident angle, the position of the scattering detector, and the orientation of the polarizers in order to adjust the fluence.

Conventional LIDT testing procedures are described in the international standards ISO 21254-1, 2, 3, and 4 [8, 9] and are briefly summarized here:

The S-on-1 procedure involves the exposure of a constant number of sites to a multiple of S laser shots at a fixed fluence. The fluence is then increased for the next set of test sites. The number of pulses passed before damage occurs is used to determine the LIDT. The damage threshold usually decreases with the number of pulses, an effect known as incubation, or fatigue [11].

The R-on-1 method, involves the irradiation of a single spot at a time while gradually increasing fluence until damage occurs. Damage can be identified in real time through the use of detection methods such as scatter detection and photothermal detection among others outlined in ISO 21254-1 [8]. This method is usually considered a less accurate approach compared with other methods due to nonlinear incubation effects associated with prolonged exposure.

The most basic technique is the 1-on-1 test in which each site in a row is irradiated with one pulse of preselected fluence. The fluence is then increased, and the process is repeated for the next row of test sites. Each site is classified as damage or undamaged. The damage probability is determined for each row as a function of fluence, and the LIDT is determined through an appropriate fit and extrapolation to zero damage probability. The form of the decline is dependent on the pulse width, with a sharp threshold in the short-pulse regime, dependent mainly on the intrinsic material properties, and a broader transition in the ns regime caused by a greater impact of defects on the damage mechanism.

2.3.2 New procedure: The results presented in this paper were obtained using a procedure similar to the 1-on-1 test, however, with 120 shots on each test site (N-on-1, N = 120). The procedure is performed at one selected wavelength and then repeated after changing the wavelength. Before the actual test, an initial R-on-1 measurement is made in order to roughly estimate the LIDT at one position on the sample by increasing fluence until a significant non-linear increase of the scatter signal is observed indicating the onset of damage. This information is then used as a guideline for the energy ranges of the following tests.

A grid of 10 × 10 test sites with a separation of 1 mm is defined for the N-on-1 test on the sample as illustrated in Figure 2 (left). Each test position in the grid was irradiated with a preselected wavelength by a fixed number of N = 120 pulses and within a given row was subjected to a fixed fluence. The fluence level was then increased or decreased for the next row using an asymptotic approach, which was found to be much more effective in finding the threshold than the conventional step increase method of ISO 21254 [8]. The first column is illuminated such that 100% of the test sites are damaged upon radiation, while the second column, contrarily, is irradiated with the aim of 0% damage status for the column. This gap between the above and below threshold fluence is gradually reduced until the threshold is reached. The procedure is illustrated in Figure 2 (right).

Both online and offline damage detection can be performed using the instrument and its ARS detector. Online detection and classification, however, requires sufficient *a priori* knowledge about the scatter threshold separating damaged from undamaged sites. For the current first studies, it was, therefore, preferred to analyze the samples after testing. For this purpose, the detector was positioned at a fixed scatter angle from the specular direction and the sample was laterally scanned in two dimensions (mapped). An important task is to find or define a scatter angle with maximum discrimination between damaged and undamaged regions. Even though not tested yet, we believe that using different scatter angles even allows for distinguishing between surface and buried defects.

Figure 3 shows the results of scatter mappings before and after damage testing. The background ARS level of about 1×10^{-3} sr^{-1} indicates areas with no significant defects and damages before and after irradiation. This scattering is caused by interface roughness of the coating and homogeneously distributed small intrinsic defects and contamination. Damaged sites after the irradiation test can easily be

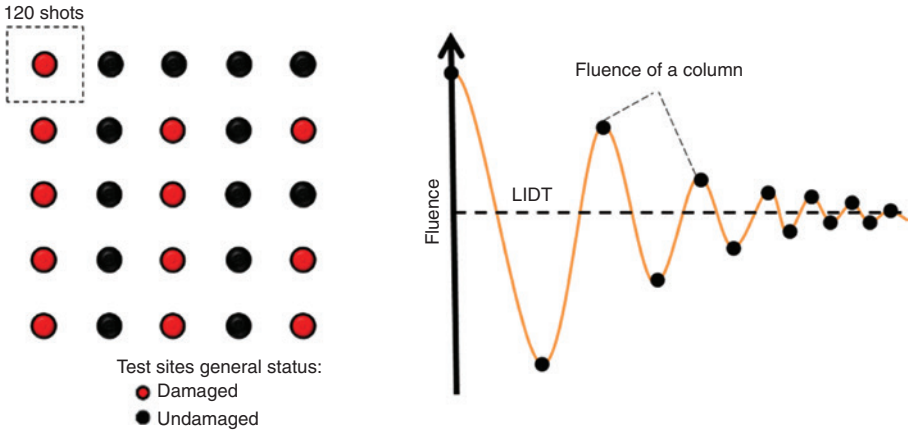

Figure 2: (Left) Schematic of typical test grid showing damaged and undamaged test sites, and (right) schematic of asymtotal method used in this investigation, approaching threshold.

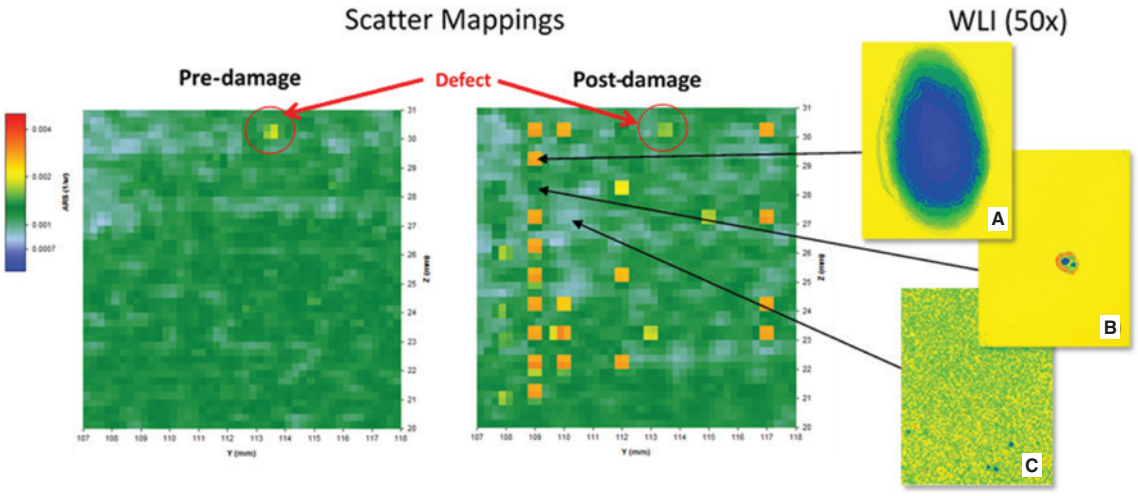

Figure 3: Left: scatter mappings on near-infrared dielectric sample of a 10 mm × 10 mm area: **pre-damage** mapping at 600 nm revealing homogeneous areas and isolated defects and **post-damage mapping** of the same area after damage testing at 600 nm. Each row corresponds to a fixed fluence. Right: White light interferometer measurements of several positions (measurement field size: 67 µm × 97 µm; z-scale: (A) –3 µm … 3 µm, (B) –0.5 µm … 0.5 µm, (C) –5 nm … 5 nm).

identified because of their substantially higher scatter levels compared to the surrounding background scattering. Shown also in the figure are white-light interferometry images taken at different test sites. The examples show a pronounced defect (a) resembling the size of the illumination spot, a small damage (b) probably corresponding to damage in its initial stage, and (c) an undamaged region. The results demonstrate that even faint damages can be detected using the light-scattering method.

For the present study, the classification of test sites was done manually based on visual inspection of the post-damage mapping. An alternative procedure would be to define a threshold ARS level slightly higher than the background. The threshold, however, would depend on the intrinsic scattering properties of the sample under study and the wavelength used. A more generalized automatic evaluation procedure could be based on calculating the difference of the images of the scatter maps after and before testing. This will be studied further in the future.

In addition, sites with preexisting defects can be located and taken into account in the analysis. This approach even has the potential to locate defects on the sample before testing and either exclude them from the LIDT test or to perform damage tests specifically on defect sites.

The current procedure for spectral damage testing is rather time consuming considering the large number of sites that have to be irradiated with different fluences and wavelengths. Testing one sample at 10 wavelengths takes about 4 h. However, because of the high degree of automatization and the possibility of an *in situ* measurement offered by the instrument, this seems to be acceptable for our first investigations and has a high potential for future optimizations.

2.3.3 Threshold determination: The post-damage mapping described above is very useful to rapidly obtain statistical information about the number of test sites damaged at a given fluence to be extracted without manually inspecting each defect

using Nomarski microscopy as usually done. The sites with a scatter level significantly higher than the average pre-damage scatter level was classified as damaged. The number of damaged sites per column corresponding to a fixed fluence divided by the total number of sites in the column is the estimated damage probability. This was then plotted against the corresponding fluence as shown in Figure 4.

As shown in Figure 4, the damage probability P_d follows a sigmoidal increase in agreement with Refs. [5] and [12]. A Boltzmann fit was adapted to account for the physical parameters involved in damage testing leading to:

$$P_d = \frac{1}{1+e^{\frac{F-F_{0.5}}{dF}}} \tag{5}$$

where $F_{0.5}$ is the fluence at which half the test sites are damaged, and dF is the width of the decline from 100% to 0% damage probability. The point of highest fluence at which P_d is approximately zero gives the estimated LIDT at the given wavelength. In the example of Figure 4, the estimated LIDT is 6 J/cm² with a rather high uncertainty of ±2 J/cm² as will be explained in Section 2.4.

In contrast to the sigmoidal transition observed, measurements in the femtosecond regime usually show a sharp decline. This illustrates that the laser stability in the nanosecond regime is heavily statistical, mainly caused by defects acting as damage precursors due to higher absorption. In Ref. [13], a model is presented that relates this sigmoidal trend to the defect distribution and standing wave electric field in multilayer HR coatings. The slope of the fitting curve, thus, contains valuable additional information about the samples.

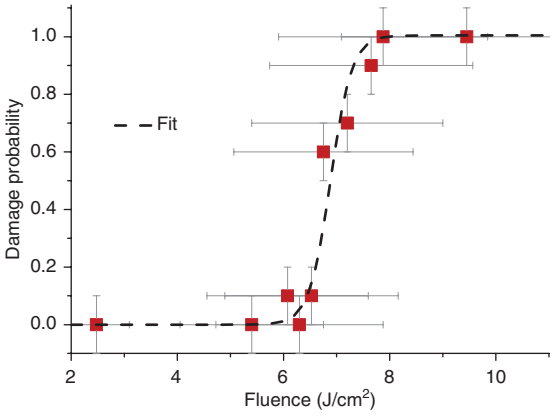

Figure 4: Damage probability as a function of fluence of a dielectric edge filter at 600 nm. Measured data and sigmoidal fit.

2.3.4 *In situ* angle-resolved light-scattering measurements: The implementation of the LIDT testing setup into an existing instrument for angle-resolved light-scattering measurements allows for a highly efficient and reproducible characterization of the samples before, during, and after damage testing. The procedure described in Section 2.3.2 is based on measuring the scattering at a fixed scatter angle, which can be chosen such that the discrimination between scattering from degradation or damage and intrinsic scattering induced, for example, by sample roughness is maximized.

As an advanced step, measuring the full angular distribution of light scattering can provide detailed information about the inner structural and optical properties of materials and coatings [14]. ARS is defined as the power scattered into a certain direction normalized to the incident power and normalized to the solid angle of detection. The main issue is, however, that the time needed for a full angular scan (about 5 min) is much longer than the irradiation time per site during our standard LIDT test. Nevertheless, the first measurements were performed to study the change of the scattering distribution during long-term irradiation as will be discussed in Section 3.2.

2.4 Uncertainty analysis

Typical sources of uncertainty in damage testing are (i) inhomogeneities and defects on the sample, (ii) debris of a damaged site spreading to a neighboring irradiation site, as well as (iii) energy fluctuations of the light source, (iv) uncertainties in the size and shape of the illumination spot on the sample, (v) uncertainties regarding damage detection and classification, and finally (vi) accumulation effects during irradiation with multiple pulses per site. For the instrument used in this study, pulse-to-pulse energy fluctuations and beam profile irregularities of the OPO light source were found to be the most critical influence factors.

Systematic studies of the beam profile performed in collaboration with the Institute of Applied Optics of the Friedrich Schiller University Jena revealed significant distortions of the spatial beam profile caused by spatial walk-off induced by the frequency conversion in the five non-linear crystals of the OPO system as well as by thermal effects (Figure 5). The non-uniform beam profile as well as the systematic change of the effective beam diameter as a function

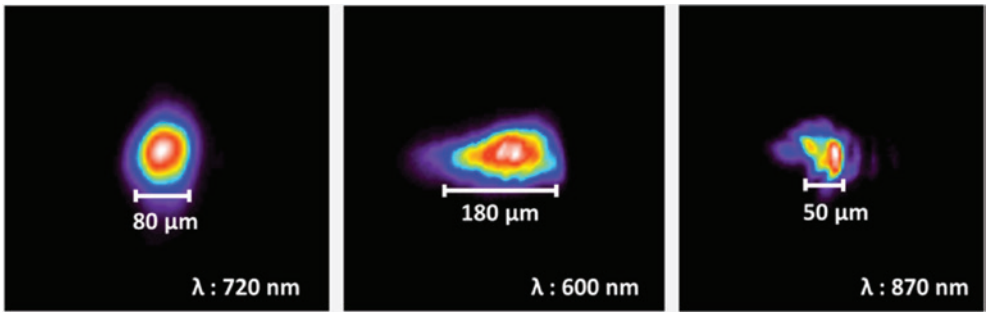

Figure 5: Beam profiles in the focal plane measured at different wavelengths revealing distortions of the beam profile and hotspots.

of the wavelength contributes to the uncertainty of measurement mainly because of possible changes of the number of defects contained in the illumination spot. Defects are known to be the main driver for laser-induced damage in the nanosecond pulse regime. Based on the morphologies of the damaged regions measured using white light interferometry, we do not believe this is a dominant effect, but a more detailed investigation will be performed in a future study. Moreover, the fluctuations of the effective beam diameter at a given wavelength have been found to be smaller than 10% and, thus, negligible in comparison to other sources of uncertainty.

Even more critical than the beam diameter issue, local hotspots were observed, which have to be assumed to lead to a systematic underestimation of the damage threshold. Online observation of the beam profile and energy made it possible to monitor these fluctuations. However, because each site was irradiated with 120 shots, energy peaks and hotspots might induce damage even if the average energy is below the actual damage threshold. The power fluctuations were found to have a standard deviation of about 20%. Therefore, the energy E_{tot} used to calculate the LIDT was taken to be the mean of the pulses above the 80th percentile of the recorded pulse energies. Accumulation effects initially were assumed to be negligible because of the rather low repetition rate of the laser operating at 20 Hz, which should allow for a sufficient dissipation of absorbed power between pulses. This, however, turned out to be not entirely true as will be discussed in Section 3.

In summary, the LIDT values determined in this study are assumed to be slightly lower than the LIDT values determined using conventional procedures and the uncertainty of the measurements estimated to be in the order of 20%.

The damage mechanisms involved in laser damage are mainly comprised of thermal processes resulting from absorption and dielectric breakdown of the material. These mechanisms vary in accordance with pulse length, repetition rate of the source, and the band gap of the material.

3 Experimental results

3.1 Spectral LIDT of metal mirrors

The damage mechanisms in the regime of 'long' pulses like the ns-pulses used in this study are primarily governed by an excess of thermal energy, which is coupled to an optical component through absorption resulting in melting and boiling [1]. This is particularly relevant for metals, and the damage properties of metals are, therefore, usually assumed to be rather simple if not trivial. Yet, predicting the spectral LIDT of metals requires detailed knowledge of the dielectric function over the entire spectral range of interest.

If the dielectric function can be assumed to be constant, simple scaling laws are sometimes used to predict the spectral damage properties. One popular example is (https://www.thorlabs.com/tutorials.cfm?tabID=762473b5-84ee-49eb-8e93-375e0aa803fa):

$$F_{th}(\lambda_2) = F_{th}(\lambda_1)\sqrt{\frac{\lambda_2}{\lambda_1}} \tag{6}$$

where $F_{th}(\lambda_2)$ is the predicted LIDT at the wavelength of interest, and $F_{th}(\lambda_1)$ is the measured LIDT at wavelength λ_1. The tendency of the LIDT to increase upon increase of wavelength is explained by the simultaneous absorption of several photons in the damage process. The more photons needed to overcome the bandgap energy of the material, the less efficient the process is. For smaller wavelengths with higher photon energy, a lower amount of photons is required to cross the gap.

Equation (6), however, has to be used with greatest caution. Almost every detailed analysis of the wavelength dependence of laser-induced damage shows strong deviations from this simple rule, for example, if the damage mechanisms change between wavelengths. Probably, the most trivial indication that the scaling rule should only be used as a guide if no other information is available is the fact that it neglects the spectral properties of the dielectric function. In order to investigate the wavelength dependence of the LIDT of a single material, aluminum mirrors, fabricated at Fraunhofer IOF (180 nm Al on superpolished silicon; Steffen Wilbrandt, Olaf Stenzel, Norbert Kaiser) with an LIDT expected to be in the range of 0.3 J/cm^2 at 1064 nm, were tested over a large spectral range.

The results of spectral LIDT measurements performed using the procedures described in Section 2 are shown in Figure 6. As expected, the LIDT decreases when going from near infrared (NIR) to shorter wavelengths. Most notable, however, is the prominent dip in the LIDT, about 800 nm. In this region, the LIDT is substantially lower than would be expected from the simple scaling law. The dip is directly linked with a known absorption feature caused by interband transitions in aluminum [15]. It is, however, to our knowledge, the first observation of such a feature in LIDT data.

The effect also has real practical consequences: The LIDT specified at one wavelength and the simple scaling law would suggest that such an aluminum mirror could be used as long as the fluence is lower than 0.1 J/cm^2, a value typical in the illumination system of our instrument. When tuning the OPO over 800 nm, however, aluminum mirrors are rapidly damaged.

An advanced empirical model to describe the spectral LIDT can be established based on Equation (6) with a correction taking into account the more complex dielectric function simply using the spectral reflectance:

$$F_{th}(\lambda_2) = F_{th}(\lambda_1)\sqrt{\frac{\lambda_2}{\lambda_1}} + B1(1 - R(\lambda_2)) + B2 \tag{7}$$

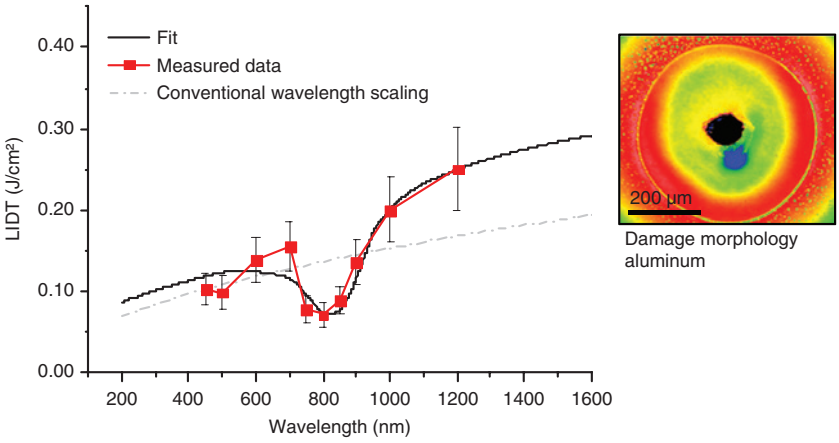

Figure 6: Spectral LIDT of aluminum mirror; the dip around 800 nm is not predicted by the simple wavelength scaling with morphology (white light interferometry) of a damage site generated at 1000 nm at a fluence of 20 J/cm² (120 shots).

where R is the reflectance, and $B1$, $B2$ are empirical factors. As shown in Figure 6, the advanced empirical model accurately describes the spectral dependence of the LIDT of the aluminum coating over the spectral range from 450 nm through 1200 nm. More detailed models based on real physical parameters can give valuable information about the damage mechanisms involved (see, for example, Ref. [3]) but are beyond the scope of this paper.

Another important question is the influence of the number of shots per site onto the estimated LIDT. Our regular LIDT testing procedure uses 120 shots per test site. Even though not expected to play a role for the low repetition rates used, the effects of the accumulation of pulses were investigated using the S-on-1 and 1-on-1 procedures at a fixed wavelength of 600 nm. The results are shown in Figure 7.

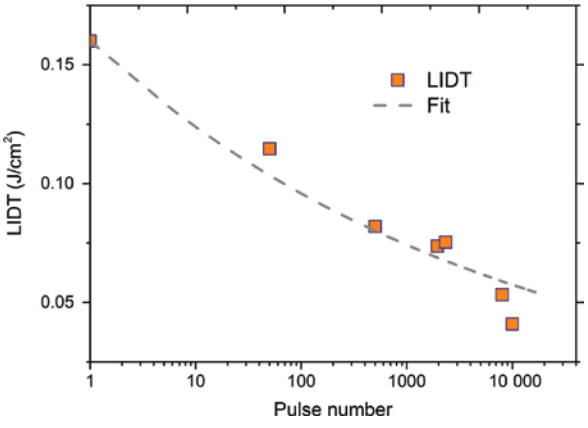

Figure 7: Results of S-on-1 and 1-on-1 testing on aluminum-coated silicon sample showing dependence of laser damage threshold on pulse number.

The LIDT decreases with increasing number of pulses per spot, the single-shot threshold, $F_{th}(1)$, being three times higher than the LIDT measured with 10^3 pulses. This effect, called incubation [16], can be attributed to the inability of the material to adequately dissipate the energy in the time between pulses even though the time between pulses of 50 ms is comparatively long. Nevertheless, the difference between the single-shot LIDT and the results obtained using 120 shots is about 20% and, thus, in the order of our general measurement uncertainty. Moreover, using an appropriate incubation model, the single-shot LIDT can be estimated based on data retrieved with higher pulse numbers. In addition to its effects on the LIDT, accumulation also had an effect on the damage morphology of the aluminum coatings starting with nanoripples [17, 18] leading to a lower LIDT for larger pulse numbers because of the increased roughness linked to greater field intensities. A detailed description of this interesting phenomenon is beyond the scope of this paper.

3.2 Spectral LIDT of dielectric interference coatings

Intrinsic material properties, roughness, and defects are well-known influence factors of laser-induced damage. The driving force for laser-induced degradation and damage, however, is the electric field of the incident light wave. Interference coatings make use of modifying the electric field distribution at the interfaces to achieve certain reflection and transmission properties. This can lead to substantial local enhancements of the electric field inside a dielectric multilayer structure resulting in damage threshold levels significantly lower than those

of the corresponding bulk materials. In Ref. [19], it was shown that the LIDT at a fixed wavelength of 1053 nm was directly proportional to the standing wave electric field maxima within the layers. Moreover, the field distribution in multilayer coatings is strongly dependent on the incident wavelength. Highly reflective coatings, for example, exhibit strong field enhancements at the interfaces, in particular, around the band edges [6]. Knowledge of the LIDT at one wavelength, usually the central wavelength of the coating, is not sufficient to describe the laser stability over the entire spectral range of application, in particular, for applications involving broadband or tunable light sources.

First, spectral damage tests were performed on an NIR edge filter with a band edge at 700 nm, which is used in our instrument to suppress IR radiation (idler) contained in the beam exiting the OPO. The requirements on the filter were (i) high transmittance (>95%) in the spectral range from 400 nm to 710 nm, (ii) low transmittance (<5%) from 710 nm to 1750 nm, (iii) low scattering (no quantitative specification), and (iv) high damage threshold (>1 J/cm^2). The filters were designed and manufactured specifically for our application at the Tongji University, Shanghai (Xinbin Cheng, Zhanshan Wang) by e-beam evaporation assisted by an RF-type ion source in order to produce dense coatings. Ta_2O_5 and SiO_2 were used as high-index and low-index materials, respectively. Superpolished fused silica substrates with a diameter of 50 mm were used.

LIDT measurements were performed using the procedure described in Section 2 at different wavelengths in the range of 600 nm and 700 nm near the band edge. The results are shown in Figure 8 together with the theoretical transmittance spectrum. The $F_{th}(\lambda)$ is about 6 J/cm^2 between 600 nm and 640 nm, significantly increasing to 9.8 J/cm^2 slightly below the band edge before sharply dropping at 700 nm below 5 J/cm^2. This is most likely related to field enhancements in this region. Strong variations of the field distribution inside interference coatings even over rather small spectral ranges were discussed, for example, in Ref. [20] as source for enhanced light scattering. An increase in the total scattering of a factor of 20 has been found for highly reflective coatings at the short-wavelength band edge compared to the central wavelength. Higher field distributions lead to lower LIDT and vice versa. Figure 8 illustrates that this effect plays an important role in laser-induced damage, and this should be studied in more detail for different types of interference coatings.

Spectral damage testing of coatings not only provides valuable information about the operating ranges of application but is also an essential tool for developing and improving coatings at the first step of production. The addition of non-quarter wave layers can help reduce the effects of standing wave electric fields in the upper more damaged prone layers of the stack as investigated by Gill et al. [21].

The strong dependence of the field distribution in interference coatings is also linked to resonant effects in the light-scattering distribution as a function of wavelength. Light scattering of high-quality interference coatings is mainly caused by the roughness and the standing field at each interface in the coating. Scattering can, thus, be used to monitor both structural and dielectric properties as well as changes of these properties during irradiation even before fatal damage. In addition to simply monitoring the scatter signal into a certain direction, measuring the ARS can provide detailed information about the coating. It has been demonstrated that, in particular, the position of so-called resonant peaks in the

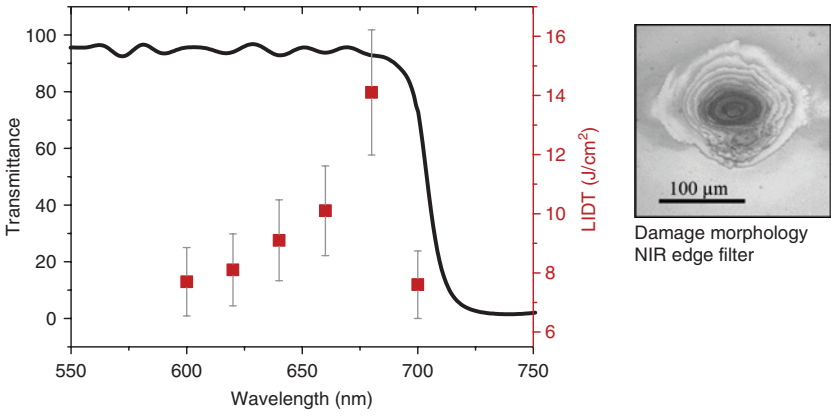

Figure 8: Spectral transmittance and LIDT about the edge of a 710-nm edge filter and morphology (Nomarski microscopy) of a single-shot damage site generated at 650 nm at a fluence of 15 J/cm^2.

scattering distribution is extremely sensitive to changes in the relationship between wavelength and optical film thickness [22].

As has been shown, accumulation of pulses at a given fluence leads to eventual damage above a certain probability level. This accumulation period, prior to the onset of ultimate damage, is not very well documented in the literature. The onset of damage in dielectric coatings can be an instantaneous event but is affected by the accumulation of pulses. It is possible that extremely small features either preexisting or induced during irradiation can act as initiators for ultimate damage. Such small features are difficult, if not impossible, to resolve with current detection methods. *In situ* ARS measurements can bridge this gap, allowing the analysis of the surface topography during the buildup of pulses and before the onset of catastrophic damage.

ARS measurements of the NIR filter were performed at wavelengths between 660 nm and 850 nm. The resulting curves shown, in part, in Figure 9 reveal resonant peaks (marked by asterisks) surrounding the specular direction (scatter angle 0°) and changing position depending on the wavelength. At each of these wavelengths, even small changes of the optical properties (optical thickness) during irradiation are assumed to lead to shifts of these resonant features. Possible increase in interface roughness or the formation of defects should lead to an increase in the scattering distribution. Thus, several aspects of laser-induced degradation can be observed by *in situ* ARS measurements. This could be very useful to study these effects even before fatal damage.

Unfortunately, the time to perform angular scattering measurements is much larger than typical irradiation times. In a first attempt, the measurement speed was increased by scanning only in the region around the resonant peaks and by reducing the integration time for each measurement point, which unavoidably resulted in increased noise in the measurements. Nevertheless, the results shown in Figure 10 for a wavelength of 670 nm reveal some interesting results.

Already for a fluence of 4 J/cm², which is well below the damage threshold of 14 J/cm² at 670 nm, a slight increase in the ARS in the measured angular range can be observed, which gradually continues to increase as the fluence gets higher. At higher fluencies, a rapid increase in the scattering can be observed, which is caused by a strong structural change or, in other words, damage. In this experiment, the rapid increase indicating damage already started at a fluence of 10 J/cm², well below the LIDT determined before using the procedure described in Section 2.3.2. This can be explained both by the longer irradiation time required for the ARS scan and the missing statistical evaluation based on the evaluation of a larger number of test sites. Unfortunately, the noise in the ARS data caused by the attempt to speed up the measurements is too strong to observe the expected angular shift of the ARS feature around –35° before the onset of fatal damage. Increasing measurement speed up to the repetition rate of the laser (20 Hz) by maintaining our usual low noise levels is one of the main goals for future studies. The approach presented in Ref. [23] is one possible way to solve this issue. Even though not fully satisfactory at this point, the results presented and discussed in this section already demonstrate the high potential of combining laser-induced damage testing with *in situ* angle-resolved light scattering measurements.

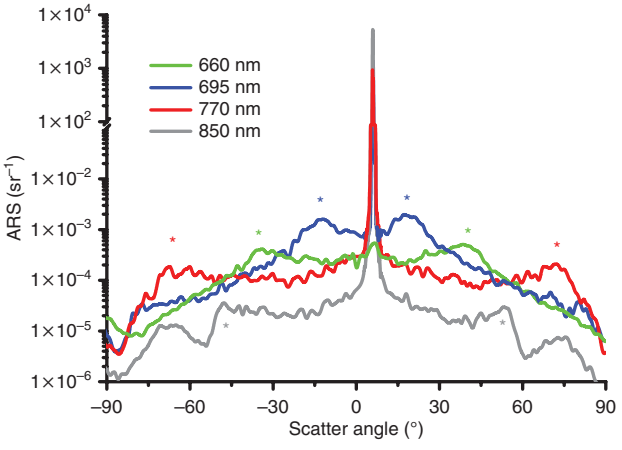

Figure 9: ARS of NIR edge filter at different wavelengths revealing resonant scattering peaks.

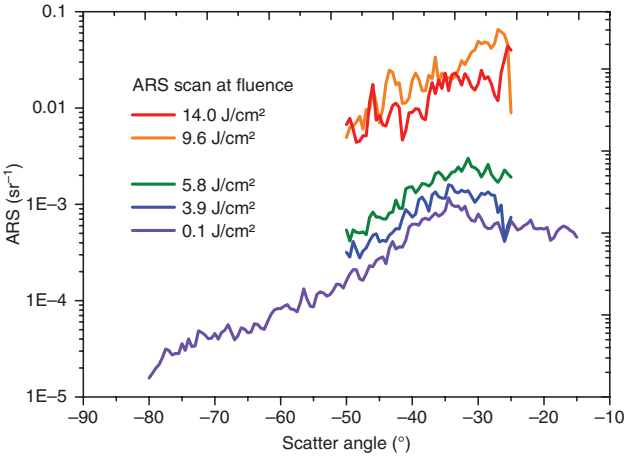

Figure 10: *In situ* ARS measurements at 670 nm of NIR edge filter at increasing fluences.

The implementation of faster methods to measure ARS could be very useful to study laser-induced degradation and damage processes in the future.

4 Summary and outlook

The laser stability of optical components is not only limited by the intrinsic absorption of the materials involved, and extrinsic factors such as defects and contaminations, but also strongly influenced by the field distribution in the components. In particular, for interference coatings, this results in a strong wavelength dependence of the laser-induced damage threshold (LIDT). Knowledge of the spectral dependence of the LIDT is of crucial importance, in particular, for the design of optical systems involving high-power broadband or tunable light sources such as OPO systems.

A new method for spectral LIDT testing has been implemented and combined with an instrument for highly sensitive ARS measurements. The instrument is based on a tunable nanosecond laser source with a tuning range from 225 nm to 1750 nm and a spectral bandwidth of less than 0.1 nm. By focusing onto the sample, fluences of up to 103 J/cm^2 can be achieved. The combination of LIDT testing with *in situ* highly sensitive ARS analysis provides additional information about structural and optical properties before, during, and after irradiation. This enables laser-induced degradation and damage processes to be studied in more detail even before fatal damage.

First, experimental studies of aluminum coatings revealed an almost linear increase in the LIDT with increasing wavelength, as roughly predicted by simple wavelength scaling laws, but also a significant dip in the LIDT around 800 nm, which is related to the spectral absorption properties of the material. This effects would be drastically underestimated when using single wavelength LIDT data and simple scaling laws and demonstrates the demand for LIDT measurements at all wavelengths relevant for the application.

For interference coatings, a rather complex wavelength dependence of the LIDT was observed, which is linked to the spectral variation of the field distribution inside the multilayer structure. For an NIR edge filter, remarkable changes of the spectral LIDT were found near the band edge. Considering the spectral field distribution in other types of coatings, drastic effects are also expected, for example, in highly reflective coatings and narrow-band filters.

Aside from broadband applications, even for single wavelength applications, knowledge of the spectral LIDT can be important considering that even small spectral shifts of the coatings or small changes of the incident angle correspond to relative changes of the wavelength of application leading to strong variations of the field distribution.

Because of the sensitivity of scattered light to both interface roughness and the field distribution, *in situ* ARS measurements can be used to monitor changes in both structural and dielectric properties during irradiation. Even though in the first tests on an NIR edge filter the expected small shift of the resonant scattering peak with increasing fluence below the damage threshold

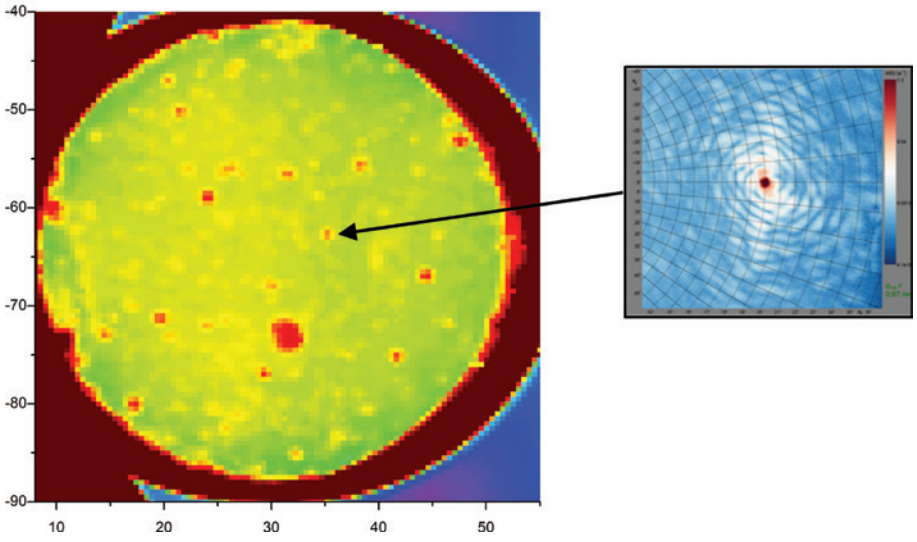

Figure 11: Scatter map of NIR edge filter measured at 640 nm. Each data point indicates the total scatter obtained from a 3D scattering distribution (left) with 3D scattering distribution of defect with a diameter of 50 μm.

could not be clearly resolved because of increased noise in the ARS data, a gradual increase in the ARS curve below threshold followed by a drastic increase and distortion above threshold could clearly be observed. This indicates a gradual growth of damage even before complete failure of the component, which might be called degradation. Moreover, we believe that even below the threshold, absorption-induced changes of the optical thickness of the coating can lead to spectral shifts resulting in enhanced fields and eventually leading to damage. Increasing ARS measurement speed and reducing noise will be the main goals for future studies to verify this assumption.

Even though they are not discussed in detail in this paper, scatter maps before and after LIDT testing can be used to study the effects of localized inhomogeneities and defects on the LIDT. The implementation of the LIDT testing setup into the instrument for spectral ARS measurements allows singular defects to be identified and classified using light scattering and then to be tested regarding their influence on the laser stability of the component.

The results of the investigations on the NIR edge filter at 640 nm before damage testing are shown in Figure 11. The scatter map reveals information on inhomogeneities and the distribution and localization of defects. The height scale is proportional to the scattering signal from the defects, which is not necessarily correlated with the defect size. More information on the dimension of the defects can be retrieved by studying the scatter distribution measured on a defect. An example of a scatter image on a defect is shown on the right in Figure 11. Analyzing the fringe structure in the scatter image suggests a defect diameter of 50 μm.

Acknowledgments: The authors gratefully acknowledge the support of the colleagues of the Fraunhofer Institute of Applied Optics and Precision Engineering for the development of the instrument, in particular, Matthias Hauptvogel and Alexander von Finck. The fruitful discussions with international experts in the field, in particular, with Lars Jensen, Istvan Balasa, and Detlev Ristau from Laser Zentrum Hannover and with Xinbin Cheng and Zhanshan Wang from Tongji University Shanghai are highly appreciated. This work was supported by the program 'Zentrales Innovations programm Mittelstand (ZIM)' of the German Ministry of Economy and Technology (BMWi), project LOSASS (ZF4023002RE6).

References

[1] L. Lamaignère, in 'Laser-Induced Damage in Optical Materials', Ed. by D. Ristau (Taylor & Francis, Boca Raton, 2015).
[2] M. Mero, J. Liu, W. Rudolph, D. Ristau and K. Starke, Phys. Rev. B 71, 115109 (2005).
[3] C. W. Carr, H. B. Radousky and S. G. Demos, Phys. Rev. Lett. 91, 127402 (2003).
[4] X. Cheng, J. Zhang, T. Ding, Z. Wei, H. Li, et al., in 'Optical Interference Coatings', Ed. by M. Tilsch and D. Ristau (OSA Technical Digest, 2013); (July 10, 2017). Available: https://www.osapublishing.org/abstract.cfm?uri=OIC-2013-FB.1.
[5] L. Gallais, J. Capoulade, J.-Y. Natoli, M. Commandré, M. Cathelinaud, et al., Appl. Opt. 47, C107-13 (2008).
[6] S. Schröder, D. Unglaub, M. Trost and A. Duparré, in 'Optical Interference Coatings', Ed. by M. Tilsch and D. Ristau (OSA Technical Digest, 2013) (July 10, 2017). Available: https://www.osapublishing.org/abstract.cfm?uri=OIC-2013-ThD.8.
[7] S. Schröder, A. Duparré, in 'Laser-Induced Damage in Optical Materials', Ed. by D. Ristau (Taylor & Francis, Boca Raton, 2015).
[8] ISO 21254, 'Lasers and Laser-Related Equipment: Test Methods for Laser-Induced Damage Threshold' (International Organization for Standardization, Geneva, Switzerland, 2011).
[9] ISO 11254, 'Laser and Laser-Related Equipment: Determination of Laser-Induced Damage Threshold of Optical Surfaces' (International Organization for Standardization, Geneva, Switzerland, 2000).
[10] B. L. Harlamoff and J. J. Jacob, 'Narrow Linewidth BBO Optical Paramateric Oscillator Utilizing Extraordinary Resonance', US 5594592 A (1995).
[11] D. Douti, L. Gallais and M. Commandré, Opt. Eng 53, 122509–122509 (2014).
[12] C. Carr, H. Radousky and S. Demos, S., Phys. Rev. Lett. 91, 127402 (2003).
[13] H. Wang, H. Qi, B. Wang, Y. Cui, M. Guo, et al., Opt. Express 23, 5213–5220 (2015).
[14] S. Schröder, T. Herffurth, H. Blaschke and A. Duparré, Appl. Opt. 50, C164–C171 (2011).
[15] H. Ehrenreich, H. Philipp and B. Segall, Phys. Rev. B 132, 1918–1928 (1963).
[16] J. Krüger, S. Martin, H. Mädebach, L. Urech, T. Lippert, et al., Appl. Surf. Sci. 247, 406–411 (2004).
[17] Z. Guosheng, P. M. Fauchet and A. E. Siegman, Phys. Rev. B 26, 5366 (1982).
[18] K. Ahmmed, C. Grambow and A. Kietzig, Micromachines 5, 1219–1253 (2014).
[19] J. Neauport, E. Lavastre, G. Razé, G. Dupuy, N. Bonod, et al., Opt. Express 15, 12508–12522 (2007).
[20] S. Schröder, D. Unglaub, M. Trost, X. Cheng, J. Zhang, et al., Appl. Opt. 53, A35–A41 (2014).
[21] D. Gill, B. Newnam and J. Mcleod, IEEE J. Quantum Electron 13, 866–867 (1977).
[22] S. Schröder, M. Trost, M. Garrick and A. Duparré, Thin Solid Films 592, 248–255 (2015).
[23] T. Herffurth, S. Schröder, M. Trost, A. Duparré and A. Tünnermann, Appl. Optics 52, 3279–3287 (2013).